A study of charged kappa in $J/\psi \to K^{\pm}K_s\pi^{\mp}\pi^0$

February 4, 2010

M. Ablikim[1], J. Z. Bai[1], Y. Bai[1], Y. Ban[11], X. Cai[1], H. F. Chen[16], H. S. Chen[1], H. X. Chen[1], J. C. Chen[1], Jin Chen[1], X. D. Chen[5], Y. B. Chen[1], Y. P. Chu[1], Y. S. Dai[18], Z. Y. Deng[1], S. X. Du[1a], J. Fang[1], C. D. Fu[1], C. S. Gao[1], Y. N. Gao[14], S. D. Gu[1], Y. T. Gu[4], Y. N. Guo[1], Z. J. Guo[15b], F. A. Harris[15], K. L. He[1], M. He[12], Y. K. Heng[1], H. M. Hu[1], T. Hu[1], G. S. Huang[1c], X. T. Huang[12], Y. P. Huang[1], X. B. Ji[1], X. S. Jiang[1], J. B. Jiao[12], D. P. Jin[1], S. Jin[1], G. Li[1], H. B. Li[1], J. Li[1], L. Li[1], R. Y. Li[1], W. D. Li[1], W. G. Li[1], X. L. Li[1], X. N. Li[1], X. Q. Li[10], Y. F. Liang[13], B. J. Liu[1d], C. X. Liu[1], Fang Liu[1], Feng Liu[6], H. M. Liu[1], J. P. Liu[17], H. B. Liu[4e], J. Liu[1], Q. Liu[15], R. G. Liu[1], S. Liu[8], Z. A. Liu[1], F. Lu[1], G. R. Lu[5], J. G. Lu[1], C. L. Luo[9], F. C. Ma[8], H. L. Ma[2], Q. M. Ma[1], M. Q. A. Malik[1], Z. P. Mao[1], X. H. Mo[1], J. Nie[1], S. L. Olsen[15], R. G. Ping[1], N. D. Qi[1], J. F. Qiu[1], G. Rong[1], X. D. Ruan[4], L. Y. Shan[1], L. Shang[1], C. P. Shen[15], X. Y. Shen[1], H. Y. Sheng[1], H. S. Sun[1], S. S. Sun[1], Y. Z. Sun[1], Z. J. Sun[1], X. Tang[1], J. P. Tian[14], G. L. Tong[1], G. S. Varner[15], X. Wan[1], L. Wang[1], L. L. Wang[1], L. S. Wang[1], P. Wang[1], P. L. Wang[1], Y. F. Wang[1], Z. Wang[1], Z. Y. Wang[1], C. L. Wei[1], D. H. Wei[3], N. Wu[1], X. M. Xia[1], G. F. Xu[1], X. P. Xu[6], Y. Xu[10], M. L. Yan[16], H. X. Yang[1], M. Yang[1], Y. X. Yang[3], M. H. Ye[2], Y. X. Ye[16], C. X. Yu[10], C. Z. Yuan[1], Y. Yuan[1], Y. Zeng[7], B. X. Zhang[1], B. Y. Zhang[1], C. C. Zhang[1], D. H. Zhang[1], F. Zhang[14f], H. Q. Zhang[1], H. Y. Zhang[1], J. W. Zhang[1], J. Y. Zhang[1], X. Y. Zhang[12], Y. Y. Zhang[13], Z. X. Zhang[11], Z. P. Zhang[16], D. X. Zhao[1], J. W. Zhao[1], M. G. Zhao[1], P. P. Zhao[1], Z. G. Zhao[16], B. Zheng[1], H. Q. Zheng[11], J. P. Zheng[1], Z. P. Zheng[1], B. Zhong[9] L. Zhou[1],

K. J. Zhu[1], Q. M. Zhu[1], X. W. Zhu[1], Y. S. Zhu[1], Z. A. Zhu[1], Z. L. Zhu[3], B. A. Zhuang[1], B. S. Zou[1]

(BES Collaboration)

[1] *Institute of High Energy Physics, Beijing 100049, People's Republic of China*

[2] *China Center for Advanced Science and Technology(CCAST), Beijing 100080, People's Republic of China*

[3] *Guangxi Normal University, Guilin 541004, People's Republic of China*

[4] *Guangxi University, Nanning 530004, People's Republic of China*

[5] *Henan Normal University, Xinxiang 453002, People's Republic of China*

[6] *Huazhong Normal University, Wuhan 430079, People's Republic of China*

[7] *Hunan University, Changsha 410082, People's Republic of China*

[8] *Liaoning University, Shenyang 110036, People's Republic of China*

[9] *Nanjing Normal University, Nanjing 210097, People's Republic of China*

[10] *Nankai University, Tianjin 300071, People's Republic of China*

[11] *Peking University, Beijing 100871, People's Republic of China*

[12] *Shandong University, Jinan 250100, People's Republic of China*

[13] *Sichuan University, Chengdu 610064, People's Republic of China*

[14] *Tsinghua University, Beijing 100084, People's Republic of China*

[15] *University of Hawaii, Honolulu, HI 96822, USA*

[16] *University of Science and Technology of China, Hefei 230026, People's Republic of China*

[17] *Wuhan University, Wuhan 430072, People's Republic of China*

[18] *Zhejiang University, Hangzhou 310028, People's Republic of China*

[a] *Currently at: Zhengzhou University, Zhengzhou 450001, People's Republic of China*

[b] *Currently at: Johns Hopkins University, Baltimore, MD 21218, USA*

[c] *Currently at: University of Oklahoma, Norman, Oklahoma 73019, USA*

[d] *Currently at: University of Hong Kong, Pok Fu Lam Road, Hong Kong*

[e] *Currently at: Graduate University of Chinese Academy of Sciences, Beijing 100049, People's Republic of China*

[f] *Currently at: Harbin Institute of Technology, Harbin 150001, People's Republic of China*

Abstract

Based on 58×10^6 J/ψ events collected by BESII, the decay $J/\psi \to K^\pm K_s \pi^\mp \pi^0$ is studied. In the invariant mass spectrum recoiling against the charged $K^*(892)^\pm$, the charged κ particle is found as a low mass enhancement. If a Breit-Wigner function of constant width is used to parameterize the kappa, its pole locates at $(849 \pm 77^{+18}_{-14}) - i(256 \pm 40^{+46}_{-22})$ MeV/c^2. Also in this channel, the decay $J/\psi \to K^*(892)^+ K^*(892)^-$ is observed for the first time. Its branching ratio is $(1.00 \pm 0.19^{+0.11}_{-0.32}) \times 10^{-3}$.

The σ and κ are controversial particles in hadron spectroscopy. They were first found in the analysis of $\pi\pi$ and πK scattering data. Because the total phase shifts in the lower mass region are much less than 180°, and they do not fit into ordinary $q\bar{q}$ meson nonets, there have been violent debates on their existence. Some recent analyses support their existence [1, 2, 3, 4, 5, 6, 7, 8, 9, 10, 11, 12].

Evidence for κ particles comes from two fields, one is from the study of production processes, and the other is from the re-analysis of the old $K\pi$ scattering data. Evidence for the κ has been found in the decay $D^+ \to K^-\pi^+\pi^-$ [8], $J/\psi \to \bar{K}^*(892)^0 K^+\pi^-$ [2, 6], $D^0 \to K^-\pi^+\mu^+\nu$ [13]. A $K\pi$ s-wave component is found in the decay $D^0 \to K^-K^+\pi^0$ [14], $D^+ \to K^-\pi^+e^+\nu_e$[15], and $\tau \to K_s\pi^-\nu_\tau$ [16]. But no evidence for the κ in $D^0 \to K^-\pi^+\pi^0$ [17] or for the charged κ in $D^0 \to K^-K^+\pi^0$ [18] is seen. The κ is found in the phenomenological analysis of $K\pi$ scattering phase shift data [19, 20, 21, 22, 23, 24, 12, 25]. However, some theorists are not convinced by the evidence for the κ [26, 27, 28, 29]. The present status of the κ is summarized by the Particle Data Group PDG [30].

The σ and κ particles have been studied with BES data, where evidence for σ and κ particles is quite clear [1, 2, 3, 4, 5, 6]. In BES, the κ was found in the decay $J/\psi \to \bar{K}^*(892)^0 K^+\pi^-$[2, 6]. In this channel, the κ is produced through $J/\psi \to \bar{K}^*(892)^0\kappa^0$, so it is a neutral κ. Because of isospin symmetry, if a neutral κ exists, there should exist a charged κ, which should be produced in $J/\psi \to \bar{K}^*(892)^\pm\kappa^\mp$. In this study, we search for and study the charged κ in $J/\psi \to K^\pm K_s\pi^\mp\pi^0$. Our analysis is based on 58 million J/ψ decays collected by BESII at the BEPC (Beijing Electron Positron Collider). The BESII detector is described in detail elsewhere [31].

In the event selection, candidate tracks are required to have a good track fit with the point of closest approach of the track to the beam axis being within the interaction region of 2 cm in r_{xy} and $\pm$20 cm in z (the beam

direction), polar angles θ satisfying $|\cos\theta| < 0.80$, and transverse momenta $P_t > 50$ MeV/c. Photons are required to be isolated from charged tracks and to come from the interaction region. Any photon with deposited energy lower than 40 MeV/c^2 in the Barrel Shower Counter (BSC) is rejected. Events are required to have four good charged tracks with total charge zero and at least two good photons.

For the reconstruction of K_s particles, we loop over all tracks, assuming them to be pions, fit the vertices of oppositely charged pairs to $K_s \to \pi^+\pi^-$, and calculate four combinations of $\pi^+\pi^-$ invariant mass, $M_{\pi\pi}$. The combination with the smallest $M_{\pi\pi}$, satisfying $|M_{\pi^+\pi^-} - M_{K_s}| < 20$ MeV/c^2 and having the decay vertex in the xy-plane satisfying $r_{xy} > 0.008$ m is kept. Time-of-flight(TOF) and dE/dx information are then used to determine whether the other two charged particles are $K^+\pi^-$ or $K^-\pi^+$.

A four constraint (4C) kinematic fit is applied under the $K^\pm\pi^\mp\pi^+\pi^-\gamma\gamma$ hypothesis, and $\chi^2_{4C} < 20$ is required. Events with a 2γ invariant mass $|M_{\gamma\gamma} - M_{\pi^0}| < 40$ MeV/c^2 are fitted with a 5C kinematic fit to $K^\pm\pi^\mp\pi^+\pi^-\pi^0$ with the two photons being constrained to the π^0 mass. Events with $\chi^2_{5C} < 50$ are selected. The combined $K^\pm\pi^0$ and $K_s\pi^\mp$ mass distribution is shown in Fig. 1(a), and the $\pi^\mp\pi^0$ mass distribution is shown in Fig. 1(b), in which the ρ resonance is clearly seen. Decay processes with an intermediate ρ state are background processes, and the requirement $|M_{\pi^\mp\pi^0} - M_\rho| > 100$ MeV/c^2 is applied to remove them. The requirements $|M_{K_s\pi^0} - 0.897| > 40$ MeV/c^2 and $|M_{K^\pm\pi^\mp} - 0.897| > 40$ MeV/c^2 are used to remove backgrounds from $J/\psi \to K^*(892)^0K^\pm\pi^\mp$ and $J/\psi \to K^*(892)^0K_s\pi^0$. The resulting scatter plot is shown in Fig. 1(e). Two clear bands, a vertical band and a horizontal band, are seen, which correspond to $J/\psi \to K^*(892)^\pm K_s\pi^\mp$ and $J/\psi \to K^*(892)^\pm K^\mp\pi^0$, respectively. The requirements $|M_{K^\pm\pi^0} - 0.892| < 80$ MeV/c^2 and $|M_{K_s\pi^\pm} - 0.892| < 80$ MeV/c^2 are imposed on the $J/\psi \to K^\pm K_s\pi^\mp\pi^0$ sample to select $J/\psi \to K^*(892)^\pm K_s\pi^\mp$ and $J/\psi \to K^*(892)^\pm K^\mp\pi^0$ events, respectively.

After the above selection, the combined $K_s\pi^\mp$ and $K^\mp\pi^0$ invariant mass distribution recoiling against the $K^*(892)^\pm$ is shown in Fig. 1(c). It is the sum of the following four decays

$$J/\psi \to K^*(892)^+K_s\pi^- \to K^+\pi^0K_s\pi^-,$$

$$J/\psi \to K^*(892)^-K_s\pi^+ \to K^-\pi^0K_s\pi^+,$$

$$J/\psi \to K^*(892)^+K^-\pi^0 \to K_s\pi^+K^-\pi^0,$$
$$J/\psi \to K^*(892)^-K^+\pi^0 \to K_s\pi^-K^+\pi^0.$$

Each decay process contributes about 1,000 events as listed in table 1. We add them together in the PWA analysis. In the spectrum shown in Fig. 1(c), a clear narrow peak at 892 MeV/c^2 and a wider peak at about 1430 MeV/c^2 are seen. In addition, there is a broad low mass enhancement just above threshold. The $K^*(892)\pi$ invariant mass distribution is shown in Fig. 1(d). Two peaks at 1270 MeV/c^2 and 1400 MeV/c^2 can be seen. The resulting Dalitz plot is shown in Fig. 1(f). The two diagonal bands correspond to the low mass enhancement combined with the peak around 892 MeV/c^2 and the peak around 1430 MeV/c^2; the horizontal band corresponds to $J/\psi \to K_1(1270)^\pm K^\mp$, $J/\psi \to K_1(1270)^0K_s$, $J/\psi \to K_1(1400)^\pm K^\mp$, and $J/\psi \to K_1(1400)^0K_s$.

Many possible sources of background are studied. First, background from K_s sidebands is studied. The $\pi^+\pi^-$ mass distribution is shown in Fig. 2(a), where a clear K_s signal can be seen and the background level is quite low. The $K\pi$ spectrum from K_s side-band events is shown in Fig. 2(b). (The K_s side-band is defined by 0.02 GeV/c^2 $< |M_{\pi\pi} - 0.497| <$ 0.04 GeV/c^2.) There are no clear structures. Next, background from π^0 sideband events is studied. The $\gamma\gamma$ spectrum is shown in Fig. 2(c), and the $K\pi$ spectrum of π^0 side-band events is shown in Fig. 2(d). (The π^0 sideband is defined by 0.04 GeV/c^2 $< |m_{\gamma\gamma} - 0.135| <$ 0.08 GeV/c^2.) There are only 120 events in Fig. 2(d), and they come from $\gamma\gamma K3\pi$, $\gamma K3\pi +$ a fake photon, and other background processes with photons in the final state. The $\gamma\gamma K3\pi$ backgrounds are very low, and the structures in Fig. 2(d) looks like those from events in the signal region and come from signal events remaining in the π^0 tails. Next, background from $K^*(892)$ side-band events is studied, and the $K^*(892)$ side-band background is shown by the dark shaded histogram in Fig. 2(e). (The $K^*(892)$ side-band is defined by 0.08 GeV/c^2 $< |M_{K\pi} - 0.892| <$ 0.16 GeV/c^2) The clear structure in the $K\pi$ mass distribution of $K^*(892)$ side-band events is the $K^*(892)$, which mainly comes the cross channel. (There are two bands in the scatter plot in Fig. 1(e). When we study one band, the other band corresponds to the cross channel.) Fig. 2(f) shows the $K\pi$ spectrum after side-band subtraction. The low mass enhancement and $K^*(892)$ peak survive after side-band subtraction.

Finally, we perform Monte Carlo simulation to study the main physics

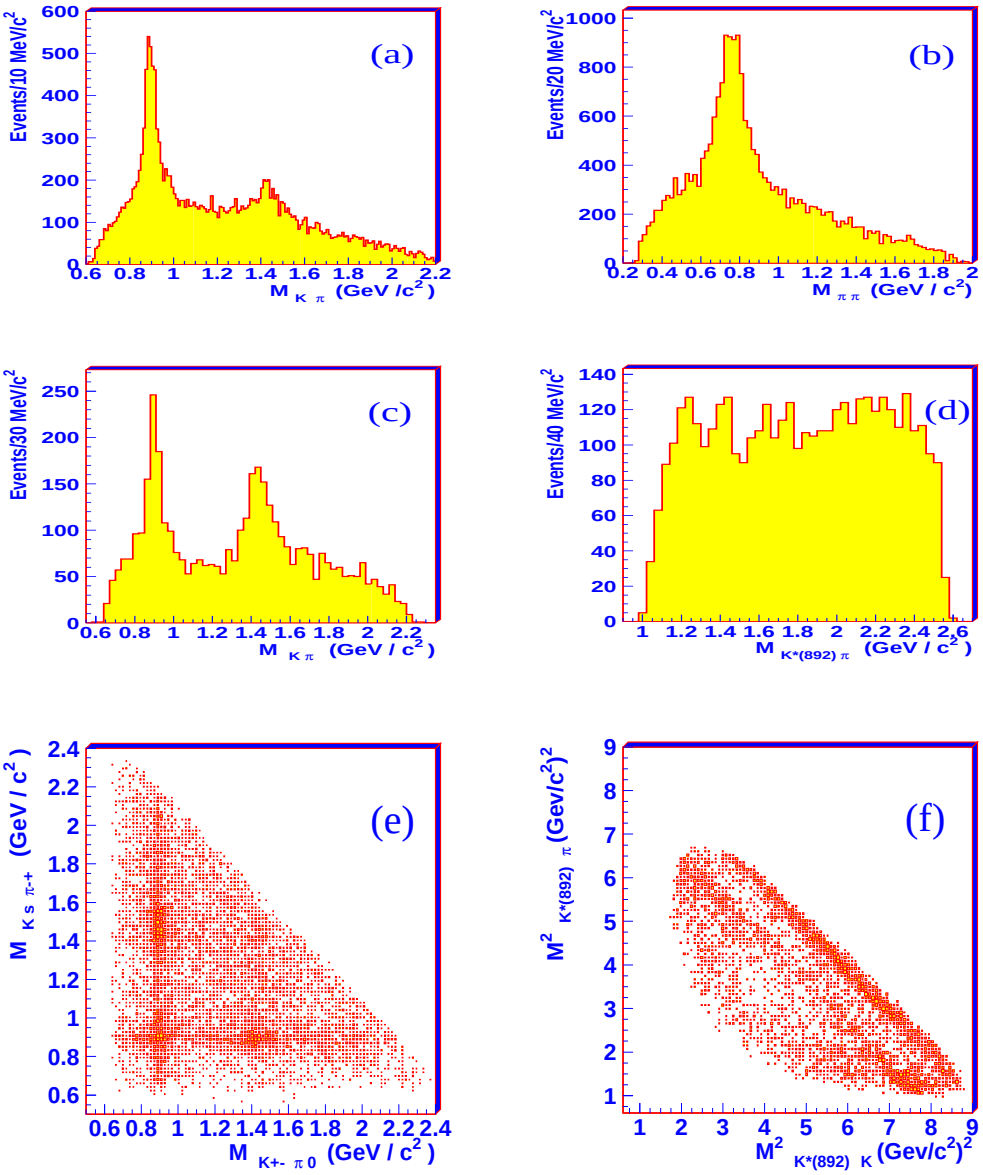

Figure 1: (a) Combined $K^{\pm}\pi^0$ and $K_s\pi^{\mp}$ mass distribution after initial cuts and ρ cuts. (b) $\pi^{\mp}\pi^0$ mass distribution. (c) Invariant mass distribution of $K^{\pm}\pi^0$ and $K_s\pi^{\pm}$ recoiling against $K^*(892)^{\mp}$. (d) Invariant mass distribution of $K^*(892)\pi$. (e) Scatter plot of $M_{K^{\pm}\pi^0}$ versus $M_{K_s\pi^{\mp}}$. (f) Dalitz plot.

background processes for this channel, including $J/\psi \to \gamma\eta_c \to \gamma K^*\bar{K}^* \to \gamma K^{\pm}K_s\pi^{\mp}\pi^0$, $J/\psi \to \gamma\eta_c \to \gamma K^*(892)^{\pm}K^{\mp}\pi^0 \to \gamma K^{\pm}K_s\pi^{\mp}\pi^0$, $J/\psi \to \gamma\eta_c \to \gamma K^*(892)^{\pm}K_s\pi^{\mp} \to \gamma K^{\pm}K_s\pi^{\mp}\pi^0$, $J/\psi \to \pi^0\pi^+\pi^-\pi^+\pi^-$, and $J/\psi \to \pi^0K^+K^-\pi^+\pi^-$. The selection efficiencies of these background processes are much lower than 1%, and the largest number of events contributed by these background processes is about 6. Therefore, the physics background is quite low.

Channel	Number of Events
$J/\psi \to K^*(892)^+K_s\pi^-$	1023
$J/\psi \to K^*(892)^-K_s\pi^+$	946
$J/\psi \to K^*(892)^+K^-\pi^0$	1055
$J/\psi \to K^*(892)^-K^+\pi^0$	1097

Table 1: Number of events from each channel. The total number of events is 4121.

After final selection, we have 4121 events. They are sum of the four decay channels, listed in Table 1. The $K\pi$ invariant mass spectrum is shown in Fig. 1(c); it is the sum of the $K_s\pi^{\pm}$ and $K^{\pm}\pi^0$ invariant mass spectra. This spectrum is quite similar to the spectrum of $K^+\pi^-$ in the decay $J/\psi \to \bar{K}^*(892)^0K^+\pi^-$ [6], which is shown in Fig. 3(b), and the spectrum of $K^{\pm}\pi^{\mp}$ and $K_s\pi^0$ in the decay $J/\psi \to K^*(892)^0K^{\pm}\pi^{\mp}$ and $J/\psi \to K^*(892)^0K_s\pi^0$, which is shown in Fig. 3(a). The biggest difference among them is that the charged $K^*(892)$ peak is much larger than the neutral $K^*(892)$ peak, which means that there are $J/\psi \to K^*(892)^{\pm}K^*(892)^{\mp}$ decays, which can be produced through J/ψ electromagnetic decays, while $J/\psi \to K^*(892)^0\bar{K}^*(892)^0$ can only be produced through J/ψ hadronic decays, which would be $SU(3)$ symmetry breaking decays and are suppressed. Fig. 3(a) is from the selection of neutral $K\pi$ modes from this channel and is also the sum of four channels. They are $J/\psi \to K^*(892)^0K^+\pi^- \to K_sK^+\pi^-\pi^0$, $J/\psi \to K^*(892)^0K^-\pi^+ \to K_sK^-\pi^+\pi^0$, $J/\psi \to K^*(892)^0K_s\pi^0 \to K_sK^+\pi^-\pi^0$, $J/\psi \to K^*(892)^0K_s\pi^0 \to K_sK^-\pi^+\pi^0$. It's shape is almost the same as the spectrum of $K^+\pi^-$ in the $J/\psi \to \bar{K}^*(892)^0K^+\pi^- \to K^-\pi^+K^+\pi^-$ decay.

A partial wave analysis, which is based on the covariant helicity amplitude

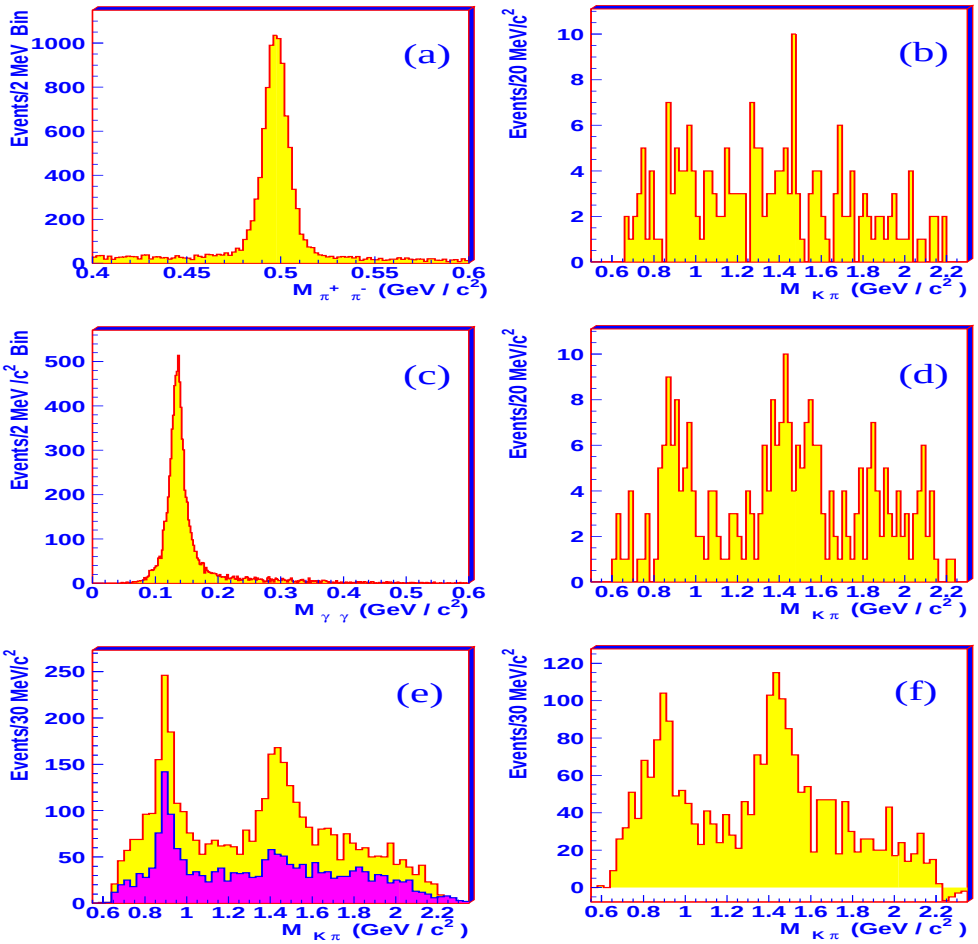

Figure 2: (a) $m_{\pi^+\pi^-}$ mass distribution after final event selection except for the K_s requirement. (b) K_s side-band structure. The K_s side-band is defined by 0.02 GeV/c^2 $< |M_{\pi\pi} - 0.497| <$ 0.04 GeV/c^2. (c) $m_{\gamma\gamma}$ mass distribution after final data selection except the π^0 requirement. (d) $M_{K\pi}$ distribution from π^0 side-band events. The π^0 sideband is defined by 0.04 GeV/c^2 $< |m_{\gamma\gamma} - 0.135| <$0.08 GeV/$c^2$. (e) $K\pi$ spectrum recoiling against $K^*(892)$. The dark shaded histogram is from K^* side-band events. The $K^*(892)$ side-band is defined by 0.08 GeV/c^2 $< |M_{K\pi} - 0.892| <$ 0.16 GeV/c^2 (f) The $K\pi$ spectrum after side-band subtraction.

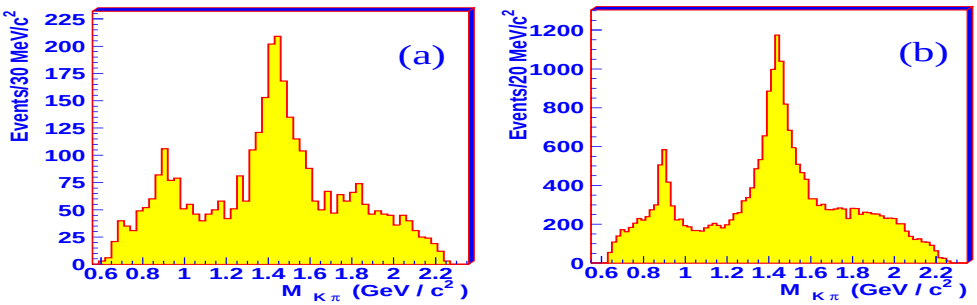

Figure 3: (a) $K\pi$ mass spectrum recoiling against neutral $K^*(892)$ in $J/\psi \to K^{\pm}K_s\pi^{\mp}\pi^0$. (b) $K\pi$ mass spectrum recoiling against neutral $K^*(892)$ in $J/\psi \to K^+K^-\pi^+\pi^-$ data [6].

analysis [33, 34, 35, 36, 37], is performed for the charged κ analysis. We add the likelihoods of all four channels together, and find the minimum of the sum of likelihood functions in the fit. We use the same method as used to fit $J/\psi \to K^*(892)^0K^+\pi^-$. The main difference is that the decay $J/\psi \to K^*(892)^{\pm}K^*(892)^{\mp}$ is included in the fit.

In the PWA analysis, ten resonances, κ, $K_0^*(1430)$, IPS, $K_2^*(1430)$, $K_2^*(1920)$, $K^*(1410)$ and $K^*(892)$ in the $K\pi$ spectrum, $K_1(1270)$ and $K_1(1400)$ in the $K^*(892)\pi$ spectrum, and $b_1(1235)$ in the $K^*(892)K$ spectrum, and two backgrounds, shown in Table 2, are considered in the fit. In Table 2, IPS refers to a broad 0^{++} structure which interferes with kappa. Its distribution in the $K\pi$ invariant mass spectrum is the same as that of phase space , so we call it Interference Phase Space (IPS). K^* BG refers to the $K^*(892)$ background coming from the cross channel. PS refers to the background with no interference with resonances. It's shape is almost the same as that of phase space, so we generally call it Phase Space background.

Three different parameterizations are used to fit the kappa. They are

$$BW_\kappa = \frac{1}{m_\kappa^2 - s - im_\kappa\Gamma_\kappa}, \qquad \Gamma_\kappa = cons., \tag{1}$$

$$BW_\kappa = \frac{1}{m_\kappa^2 - s - i\sqrt{s}\Gamma_\kappa(s)}, \qquad \Gamma_\kappa(s) = \frac{g_\kappa^2 \cdot k_\kappa}{8\pi s}, \tag{2}$$

$$BW_\kappa = \frac{1}{m_\kappa^2 - s - i\sqrt{s}\Gamma_\kappa(s)}, \qquad \Gamma_\kappa(s) = \alpha \cdot k_\kappa, \tag{3}$$

Resonance	Spin-Parity	Decay Mode	Mass (MeV//c^2)	Width (MeV/c^2)	Sig.
κ (1)	0^+	$K\pi$	$810 \pm 68^{+15}_{-24}$	$536 \pm 87^{+106}_{-47}$	$> 6\sigma$
κ (2)	0^+	$K\pi$	$884 \pm 40^{+11}_{-22}$	$478 \pm 77^{+71}_{-41}$	$> 6\sigma$
κ (3)	0^+	$K\pi$	$1165 \pm 58^{+120}_{-41}$	$1349 \pm 500^{+472}_{-176}$	$> 6\sigma$
$K_0^*(1430)$	0^+	$K\pi$	1400 ± 86	325 ± 200	0.6σ
IPS	0^+	$K\pi$	—	—	$> 6\sigma$
$K_2^*(1430)$	2^+	$K\pi$	1411 ± 30	111 ± 46	$> 6\sigma$
$K_2^*(1920)$	2^+	$K\pi$	2020 ± 140	705 ± 160	$> 6\sigma$
$K^*(1410)$	1^-	$K\pi$	1420 ± 14	130 ± 28	$> 6\sigma$
$K^*(892)$	1^-	$K\pi$	896 ± 8	57 ± 12	$> 6\sigma$
$K_1(1270)$	1^+	$K^*(892)\pi$	1254 ± 14	60 ± 28	$> 6\sigma$
$K_1(1400)$	1^+	$K^*(892)\pi$	1390 ± 30	146 ± 44	$> 6\sigma$
$b_1(1235)$	1^+	$K^*(892)K$	1230 ± 52	142 ± 38	4.5σ
$K^*(892)$ BG	1^-	$K\pi$	—	—	$> 6\sigma$
PS BG	—	—	—	—	—

Table 2: Resonances included in the fit of this channel. Masses and widths of various resonances are determined by mass and width scans. κ (1), (2) and (3) are results given by fits using Breit-Wigner functions (1), (2) and (3) to fit κ respectively. IPS refers to the broad 0++ structure which interferes with kappa. K^* BG refers to the $K^*(892)$ background coming from the cross channel. PS BG refers to the background with no interference with resonances.

where k_κ is the magnitude of the momentum of the K in the $K\pi$, or the κ center of mass system [38], and α is a constant which will be determined by fit. Parameters in the Breit-Wigner function are determined by mass and width scans. Our fit method is: find a global minimum first, then make mass and width scans. The procedure is repeated until solutions no longer change. In the mass and width scans, we fix masses, widths, and amplitudes of all other resonances. For the Breit-Wigner function of constant width, i.e. equation (1) to fit κ, the scan curves are shown in Fig. 4. The minima of the curves gives the central values of mass and width parameters for equation (1). The corresponding mass and width parameters for the other two Breit-Wigner functions are obtained in the same way. From the mass and width parameters, the corresponding pole positions can be directly calculated from equation (1), (2) and (3). Our final results are listed in the Table 3, where the first errors are statistical, and the second are systematic. The mass and width parameters obtained by different parameterizations are quite different, but their poles are almost the same. This situation is quite similar to what we found in the study of the neutral κ. The corresponding results for the neutral κ [6] are shown in Table 4. The results for the charged κ are consistent with those of the neutral κ. For the systematic uncertainties, the following are included: the effect of multi-solutions, the effect of removing $K_0(1430)$, IPS, $b_1(1235)$ and $K^*(892)\bar{K}^*(892)$, the result of a fit with the $K^*(892)$ background level floating, and the result from a fit using direct side-band subtraction.

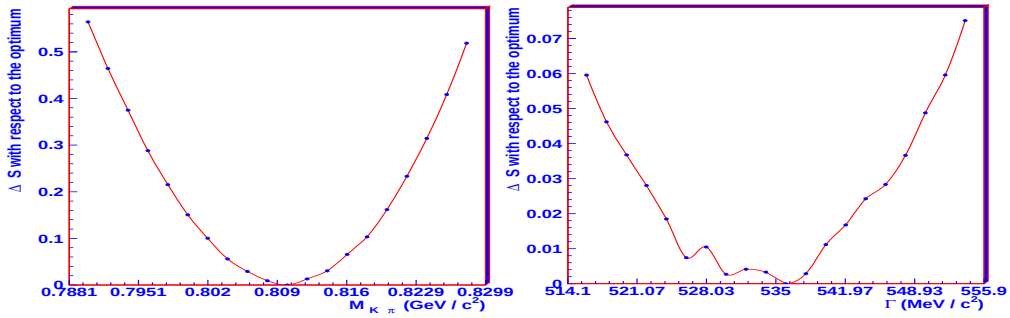

Figure 4: Mass and width scan for the charged kappa, using a Breit-Wigner function of constant width. The left figure shows the mass scan curve, and the right figure shows the width scan curve.

	BW (1)	BW (2)	BW (3)
Mass (MeV/c^2)	$810 \pm 68^{+15}_{-24}$	$884 \pm 40^{+11}_{-22}$	$1165 \pm 58^{+120}_{-41}$
Width (MeV/c^2)	$536 \pm 87^{+106}_{-47}$	$478 \pm 77^{+71}_{-41}$	$1349 \pm 500^{+472}_{-176}$
pole (MeV/c^2)	$(849 \pm 77^{+18}_{-14})$ $-i(256 \pm 40^{+46}_{-22})$	$(849 \pm 51^{+14}_{-28})$ $-i(288 \pm 101^{+64}_{-30})$	$(839 \pm 145^{+24}_{-7})$ $-i(297 \pm 51^{+50}_{-18})$

Table 3: Masses, widths and pole positions of the charged κ. In the table, the first errors are statistical, and the second are systematic. BW (1) means equation (1) is used to fit the κ. BW (2) and BW (3) have similar meanings.

	BW (1)	BW (2)	BW (3)
Mass (MeV/c^2)	$745 \pm 26^{+14}_{-91}$	$874 \pm 25^{+12}_{-55}$	$1140 \pm 39^{+47}_{-80}$
Width (MeV/c^2)	$622 \pm 77^{+61}_{-78}$	$518 \pm 65^{+27}_{-87}$	$1370 \pm 156^{+406}_{-148}$
pole (MeV/c^2)	$(799 \pm 37^{+16}_{-90})$ $-i(290 \pm 33^{+25}_{-38})$	$(836 \pm 38^{+18}_{-87})$ $-i(329 \pm 66^{+28}_{-46})$	$(811 \pm 74^{+17}_{-83})$ $-i(285 \pm 20^{+18}_{-42})$

Table 4: Masses, widths and pole positions of the neutral κ [6]. BW (1) means equation (1) is used to fit the κ. BW (2) and BW (3) have similar meaning.

Our final results correspond to the solution with the minimum least likelihood. Differences amongst solutions with similar likelihood values are also included as systematic uncertainties. The masses and widths of all resonances obtained by mass and width scans are shown in the Table 2. In the fit, we find the contribution from $K_0^*(1430)$ to be small; it's statistical significance is only 0.6σ. Because it is expected in this channel, we include it in the final solution. The statistical significances of all other resonances are above 6σ. The final fit of $K\pi$ spectrum is shown in Fig. 5(a), where points with error bars are data, and the light shaded histogram is the final fit. In the figure, the dark shaded histogram shows the contribution of the charged κ. Fig. 5(b) shows the final fit for the $K^*(892)\pi$ spectrum. Fig. 6 shows the final fit for the angular distributions, and Fig. 7 shows contributions of some main resonances.

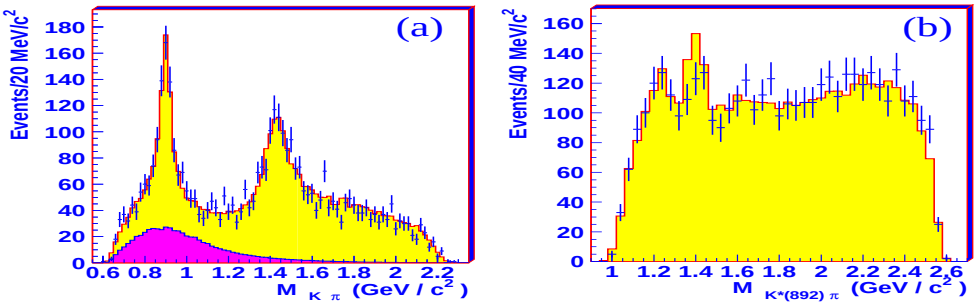

Figure 5: (a) Final fit results for the $K\pi$ spectrum. Points with error bars are data, the light shaded histogram is the final global fit, and the dark shaded histogram is the contribution of the kappa. (b) Final fit of $K^*(892)\pi$ spectrum. Dots with error bars are data, and the histogram is the final global fit. There are two peaks in the lower mass region. The lower one is fit by the $K_1(1270)$, and the higher one is by the $K_1(1400)$. They are 1^+ resonances.

In the final solution, the decay $J/\psi \to K^*(892)^\pm\kappa^\mp$ contributes 655 events. Monte-Carlo simulation of the decay $J/\psi \to K^*(892)^\pm\kappa^\mp \to K^\pm K_s\pi^\mp\pi^0$ determines an efficiency of 2.33%, and the branching ratio of $J/\psi \to K^*(892)^+\kappa^-$ or $J/\psi \to K^*(892)^-\kappa^+$ is

$$BR = \frac{655/4}{2.33\% \times 5.8 \times 10^7 \times 1/9} = (1.09 \pm 0.18^{+0.94}_{-0.54}) \times 10^{-3}, \qquad (4)$$

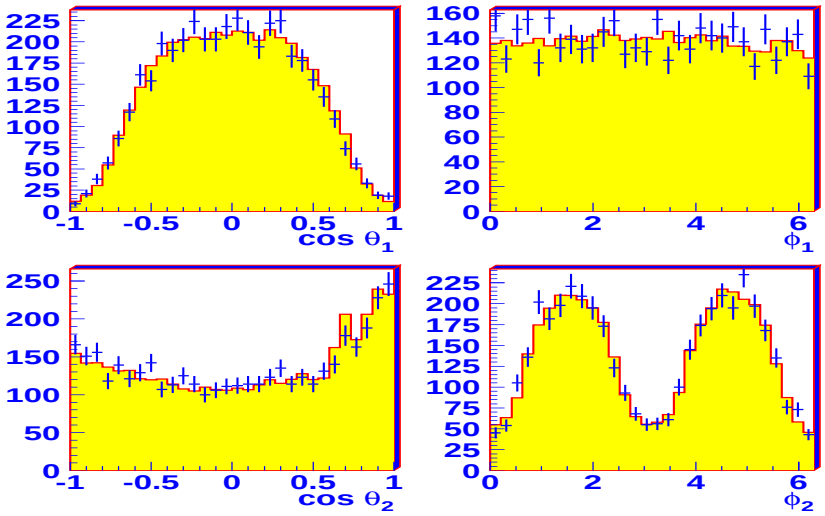

Figure 6: Final fit result for the angular distributions. Dots with error bars are data, and the histogram is the final global fit. The upper left figure shows the final fit of the θ_1 distribution, the upper right shows the final fit of the ϕ_1 distribution, the lower left shows the final fit of the θ_2 distribution, the lower right shows the final fit of the ϕ_2 distribution. θ_1 and ϕ_1 are the polar angle and azimuthal angle of the $K\pi$ system in the J/ψ center of mass system. θ_2 and ϕ_2 are the polar angle and azimuthal angle of the K meson in the $K\pi$ center of mass system.

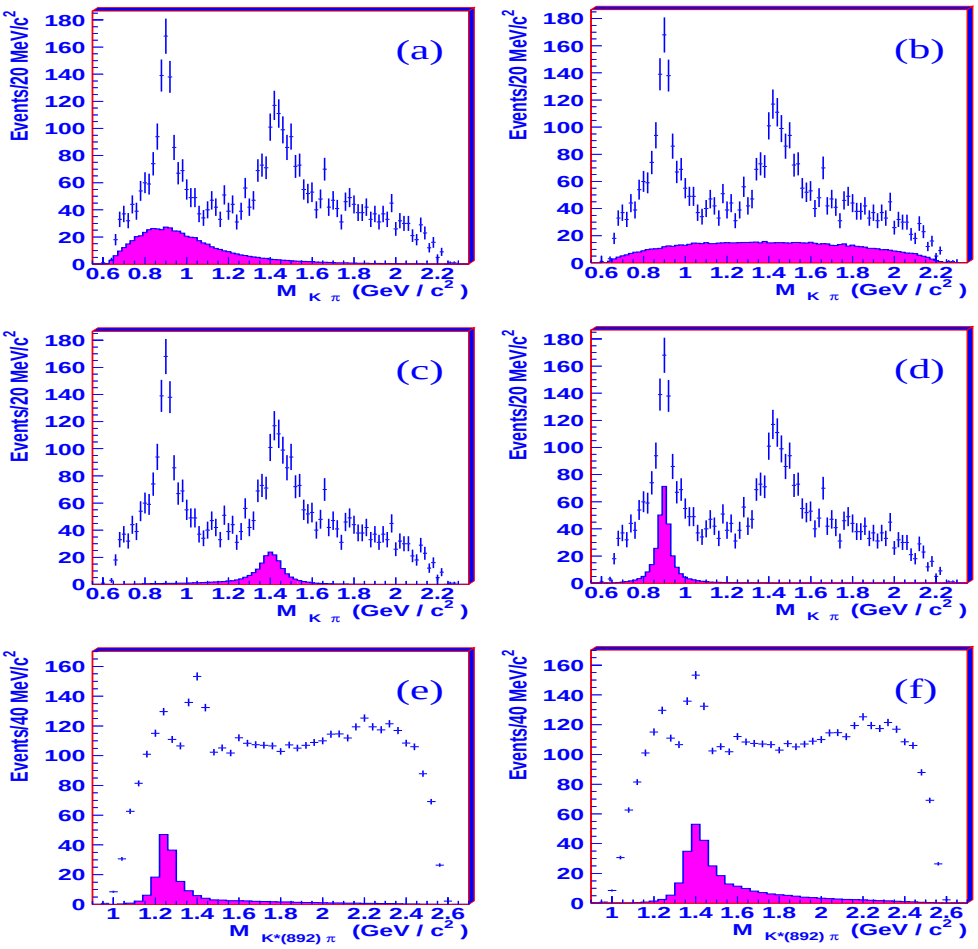

Figure 7: Contributions from various resonances. (a) κ, (b) contribution from IPS, (c) $K_2^*(1430)$, (d) $K^*(892)$, (e) $K_1(1270)$, (f) $K_1(1400)$. The last two figures are distributions of $K^*(892)\pi$, and others are distributions of $K\pi$. In these figures, dots with error bars are data, and the histograms are the contributions of the corresponding resonance.

where, the first error is statistical, the second error is systematic, the factor $\frac{1}{4}$ is because the events are the sum of four channels, and the factor $\frac{1}{9}$ is the isospin factor. In the previous study of the decay $J/\psi \to \bar{K}^*(892)^0 K^+\pi^-$, the corresponding branching ratio for the neutral κ is $(0.52 - 0.97) \times 10^{-3}$[39]. The two results are consistent with that expected from isospin symmetry. The systematic error contains the following contributions: uncertainties from multi-solutions, from different fit method to backgrounds, and from removing some components from fit($K_0^*(1430)$, IPS, $B_1(1235)$, and $K^*(892)^{\pm}K^*(892)^{\mp}$).

Also interesting in this channel is the existence of the J/ψ electromagnetic decay $J/\psi \to K^*(892)^{\pm}K^*(892)^{\mp}$. In fact, the peak at 892 MeV/c^2 in the $K\pi$ invariant mass spectrum (see Fig. 1(c)) comes from two sources: one source is from the cross channel, the other is from $J/\psi \to K^*(892)^{\pm}K^*(892)^{\mp}$ decay. The number of events from the cross channel can be calculated approximately from the $K^*(892)$ side-band structure. Fig. 2(e) shows the $K^*(892)$ side-band structure, and Fig. 2(f) shows the $K\pi$ invariant mass spectrum after side-band subtraction. In this figure, the narrow peak at 892 MeV/c^2 is clear. In the final fit, the decay $J/\psi \to K^*(892)^{\pm}K^*(892)^{\mp}$ contributes 323 events. The Monte-Carlo simulation of the decay $J/\psi \to K^*(892)^{\pm}K^*(892)^{\mp} \to K^{\pm}K_s\pi^{\mp}\pi^0$ yields an efficiency of 1.25%, and the branching ratio of $J/\psi \to K^*(892)^+K^*(892)^-$ is

$$BR = \frac{323/2}{1.25\% \times 5.8 \times 10^7 \times 1/9 \times 2} = (1.00 \pm 0.19^{+0.11}_{-0.32}) \times 10^{-3}, \quad (5)$$

where, the first error is statistical, the second error is systematic, the factor $\frac{1}{2}$ is because events are counted twice, the factor $\frac{1}{9}$ is the isospin factor, and the factor 2 is because the data comes from two decay channels:

$$J/\psi \to K^*(892)^+K^*(892)^- \to (K^+\pi^0)(K_s\pi^-)$$

and

$$J/\psi \to K^*(892)^-K^*(892)^+ \to (K^-\pi^0)(K_s\pi^+).$$

The systematic error contains the following contributions: uncertainties from multi-solutions, from different fit method to backgrounds, and from removing some components from fit($K_0^*(1430)$, IPS, and $B_1(1235)$).

In conclusion, the charged κ is observed and studied in the decay $J/\psi \to K^*(892)^{\pm}\kappa^{\mp} \to K^{\pm}K_s\pi^{\mp}\pi^0$. The low mass enhancement in the $K\pi$ spectrum

can not be fit well unless a charged κ is added into the solution. If we use a Breit-Wigner function of constant width to parameterize the kappa, its pole locates at $(849 \pm 77^{+18}_{-14}) - i(256 \pm 40^{+46}_{-22})$ MeV/c^2. In our analysis, three different parameterizations are tried in the fit, and final results are shown in Table 3 and are consistent with those of the neutral κ and are also in good agreement with those obtained in the analysis of $K\pi$ scattering phase shifts. Also, in this channel, the decay $J/\psi \to K^*(892)^{\pm}K^*(892)^{\mp}$ is observed for the first time with the branching ratio $(1.00 \pm 0.19^{+0.11}_{-0.32}) \times 10^{-3}$. The corresponding decay mode is not observed in $J/\psi \to \bar{K}^*(892)^0 K^+\pi^-$.

Acknowledgments The BES collaboration thanks the staff of BEPC and computing center for their hard efforts. This work is supported in part by the National Natural Science Foundation of China under contracts Nos. 10491300, 10225524, 10225525, 10425523, 10625524, 10521003, 10821063, 10825524, the Chinese Academy of Sciences under contract No. KJ 95T-03, the 100 Talents Program of CAS under Contract Nos. U-11, U-24, U-25, and the Knowledge Innovation Project of CAS under Contract Nos. U-602, U-34 (IHEP), the National Natural Science Foundation of China under Contract Nos. 10775077, 10225522 (Tsinghua University), and the Department of Energy under Contract No. DE-FG02-04ER41291 (U. Hawaii).

References

[1] Ning Wu (BES collaboration), "BES R measurements and J/ψ Decays", Proceedings of the XXXVIth Rencontres de Moriond, Les Arcs, France, March 17 – 24, 2001, Ed. J. Tran Thanh Van. 2001 QCD and High Energy Hadronic Interactions, p.3-6.

[2] J.Z.Bai, BES Collaboration, hep-ex/0304001.

[3] J.Z.Bai, et al., BES collaboration, High Energy Phys. Nucl. Phys. 28 (2004) 215.

[4] M. Ablikim, et al., BES collaboration, Phys. Lett. **B 598** (2004) 149.

[5] M. Ablikim, et al., BES collaboration, Phys. Lett. **B 645** (2007) 19.

[6] M. Ablikim, et al., BES collaboration, Phys. Lett. **B 633** (2006) 681.

[7] E.M. Aitala, et al., Fermilab E791 Collaboration, Phys. Rev. Lett. 86 (2001)770.

[8] E.M. Aitala, et al., Fermilab E791 Collaboration, Phys. Rev. Lett. 89 (2002)121801.

[9] D. Alde, et al., Phys. Lett **B 397** (1997) 350.

[10] T. Ishida, et al., in: Proceedings of International Conference Hadron'95, World Scientific, Manchester, UK, 1995.

[11] V.E. Markushin, M.P. Locher, Frascati Phys. ser. 15 (1999) 229.

[12] Z.Xiao, H.Q.zheng, Nucl. Phys. A 695 (2001) 273.

[13] J.M. Link, et al., FNAL FOCUS Collaboration, Phys. Lett. **B535** (2002)430.

[14] C. Cawlfield, et al., CLEO Collaboration, Phys. Rev. **D 74** (2006) 031108R.

[15] M.R. Shepherd, et al., CLEO Collaboration, Phys. Rev. **D 74** (2006) 052001.

[16] D. Epifanov, et al., BELLE Collaboration, Phys. Lett. **B 654** (2007) 65.

[17] S. Anderson, et al., Phys. Rev. **D 63** (2001)09001.

[18] B. Aubert, et al., BABAR Collaboration, Phys. Rev. **D 76** (2007) 011102R.

[19] E. van Beveren, et al., Z. Phys. **C 30** (1986)651.

[20] D. Aston, et al., Nucl. Phys. **B 296** (1988)253.

[21] S. Ishida, et al., Prog. Theor. Phys. **98** (1997)621.

[22] D.Black, et al., Phys. Rev. **D58** (1998)054012

[23] J.A. Oller, E. Oset, Phys. Rev. **D 60** (1999)074023.

[24] M.J. Jamin, et al., Nucl. Phys. **B 587** (2000)331.

[25] D. Bugg, Phys. Lett. **B 572** (2003)1.

[26] D. Lohs, Phys. Lett. **B 234** (1990)235.

[27] N.A. Tornqvist, Z. Phys. **C 68** (1995) 467.

[28] A.V. Anisovich, A.V. Sarantsev, Phys. Lett. **B 413** (1997) 137.

[29] S.N. Cherry, M.R. Pennington, Nucl. Phys. **A 688** (2001) 823.

[30] Priticle Data Group, Phys. Lett. **B 667** (2008) 1.

[31] J.Z. Bai, et al., BES Collaboration, Nucl. Instrum. Methods, **A** 344 (1994)319; J.Z. Bai, et al., BES Collaboration, Nucl. Instrum. Methods, **A** 458 (2001)627.

[32] H.Q.Zheng, et al., Nucl. Phys. **A 733** (2004) 235.

[33] M. Jacob, G.C. Wick, Ann.Phys. (NY) **7** 404 (1959).

[34] S.U.Chung, Phys. Rev. D57, 1998:431-442.

[35] Ning Wu and Tu-Nan Ruan, Commun. Theor. Phys. (Beijing, China) **35** (2001) 547.

[36] Ning Wu and Tu-Nan Ruan, Commun. Theor. Phys. (Beijing, China) **35** (2001) 693.

[37] Ning Wu and Tu-Nan Ruan, Commun. Theor. Phys. (Beijing, China) **37** (2002) 309.

[38] H.Q. Zheng, *How to parameterize a resonance with finite width* , Talk given at International Symposium on Hadron Spectroscopy, Chiral Symmetry and Relativistic Description of Bound Systems, Tokyo, Japan, 24-26 Feb 2003; hep-ph/0304173.

[39] The branching ratio of the neutral kappa was not reported in Ref. [6]. In the study of the neutral kappa, the number of kappa events was in the range 1891 - 3516, and the selection efficiency was 14.2%. Its branching ratio is $\frac{1891-3516}{14.2\%\times 5.8\times 10^7\times 4/9} = (0.52 - 0.97)\times 10^{-3}$